Evaluation of a Limited-area Energy Budget Cycle of an Extratropical Storm Under Lagrangian and Eulerian Frameworks

Sébastien Rougerie-durocher (sebrdurocher@gmail.com)
IRDA: Institut de recherche et de developpement en agroenvironnement https://orcid.org/0000-0002-9585-2091

René Laprise
UQAM: Universite du Quebec a Montreal

Oumarou Nikiéma
Environnement Canada: Environment and Climate Change Canada

Research Article

Keywords: Energy Budget, Eulerian and Lagrangian coordinate system, Limited-Area Domain, Regional Climate Model, North American Climate

Posted Date: March 23rd, 2021

DOI: https://doi.org/10.21203/rs.3.rs-315207/v1

Title: Evaluation of a limited-area energy budget cycle of an extratropical storm under Lagrangian and Eulerian frameworks

Authors: Sébastien Rougerie-Durocher[a,b], René Laprise[b], Oumarou Nikiéma[c]

Affiliations:

[a] Institute of Research and Development in Agroenvironment, Saint-Bruno-de-Montarville, QC J3V 0G7, Canada

[b] Centre ESCER, Department of Earth and Atmospheric Science, UQAM, Montréal, QC H3C 3P8, Canada

[c] Environment and Climate change Canada, Dorval, QC, Canada

Corresponding author address:

Sébastien Rougerie-Durocher
Institute of Research and Development in Agroenvironment,
Saint-Bruno-de-Montarville, QC, Canada J3V 0G7
Email: sebrdurocher@gmail.com

Abstract: To conceptualize the uncertainties regarding the mechanisms of extratropical cyclones (EC), a study of their energy cycle can provide key information of their fundamental structure. This study applies a set of equations built from earlier works for a limited-area energy decomposed into temporal mean and deviations. It compares the results obtained with a reference frame that tracks an EC through its eddy kinetic energy with those obtained with a larger but fixed frame. A specific storm that occurred throughout the period of December 10-18th 2004 and simulated by the Canadian Regional Climate Model (CRCM – version 5) was studied. Results support the notion that the moving reference results in larger amplitudes for all temporal deviation components of the cycle than for the fixed reference. A time tendency analysis of the energetic reservoirs reveals noteworthy phases in the storm's energy, with an increase and decrease occurring during the periods of 10-14 December and 14-18 December, respectively. The energy budget is overall fairly well balanced, with the exception of a lateral boundary term, $h_{k_{TV}}$, with considerable negative

values; this term exhibits a spatially larger scale than the other contributions in the EC. An evaluation of the sensibility of the tracking scheme related to its size and positioning was also performed to determine its influence on the boundary term $h_{k_{TV}}$.

Keywords: Energy Budget, Eulerian and Lagrangian coordinate system, Limited-Area Domain, Regional Climate Model, North American Climate

Declarations:

Funding: This research was funded by the Discovery grant Program of the Natural Sciences and Engineering Research Council of Canada (NSERC; http://www.nserc-crsng.gc.ca) and the project "Marine Environmental Observation, Prediction and Response" (MEOPAR; http://meopar.ca) of the Networks of Centres of Excellence (NCE; http://www.nce-rce.gc.ca) of Canada.

Conflict of interest: The authors have no conflicts of interest to declare that are relevant to the content of this article

Availability of data and material: Not available

Code availability: Not available

Acknowledgements: The calculations were performed by the Guillimin supercomputer of Compute Canada – Calcul Québec. The authors thank Mr. Georges Huard, Mrs. Katja Winger and Mrs. Nadjet Labassi for maintaining an efficient and user-friendly local computing facility.

1. Introduction

An important role of the atmosphere is that of a thermal machine redistributing energy to compensate the meridional gradient of incoming energy caused by the inclination of the incident solar radiation across latitudes (Lorenz 1967). Amongst the atmospheric processes that contribute to the meridional redistribution of energy, extratropical cyclones (EC) are considered as playing a pivotal role (Starr and White 1951; Starr 1953 and 1954; Fjortoft 1951). It has been noted, both numerically and through observations, that EC undergo a lifecycle that can best be understood in terms of an atmospheric energy cycle (Ulbrich and Speth 1991). The benefits of using atmospheric energy cycles are twofold. First, it allows a better understanding of how EC redistribute the energy, by depicting the cyclones energy conversions. Second, it allows improvements in weather predictions and climate simulations as the various weaknesses of weather and climate models can become manifest when studying their energetics (Boer and Lambert 2008).

Numerous atmospheric energetic studies have been carried out, starting with Margules (1905; see also Tamura 1905) who notably introduced the notion of total potential energy (TPE) and its subsequent conversion to kinetic energy (KE). This approach served as basis for Lorenz's own derivation (Lorenz 1955, 1967) for a global atmospheric energy cycle that is considered as the foundation for the many formulations that exist today. Lorenz identified the dynamically active component of Margules' TPE as being the available potential energy (APE), its magnitude being proportional to the difference between a notional barotropic reference state and the state of the atmosphere at any given time. He then separated APE and KE into zonal mean and deviations to adequately distinguish zonally symmetric circulations phenomena such as the Hadley cell from travelling disturbances such as extratropical cyclones.

The atmospheric general circulation is mostly driven by differential diabatic heating that generates zonal available potential energy (ZAPE) and its conversion to its eddy component (EAPE) through disturbances in the westerlies that accomplish meridional transport of sensible heat. Rising/sinking of warm/cold air within a latitude belt accompanies meridional transport of heat, which converts EAPE into eddy kinetic energy (EKE). This EKE is then either dissipated or transformed into zonal

kinetic energy (ZKE) by barotropic processes occurring mainly in the stage of cyclolysis (Kuo 1951; Starr and White 1951; van Mieghem 1952). Oort (1964) was the first to quantify Lorenz's cycle for annual-mean conditions over the northern hemisphere.

Following Lorenz's seminal work, numerous studies have been carried out to examine the energy of the atmosphere (van Mieghem 1955; Wiin-Nielsen 1967; Peixoto and Oort 1974; Michaelides 1987, Yeon and Maeng 2013; to name just a few). By using Lorenz's theory, Oort (1964) and Dutton and Johnson (1967) have shown the importance of baroclinic conversion in the development of storms, which curtailed an earlier hypothesized importance of barotropic conversion (Smith 1969).

In today's climate research, atmospheric energy budgets have proven themselves to be pertinent tools (O'Gorman and Schneider 2008) especially when attempting to target EC (Muench 1965; Smith 1969; Johnson 1970; Marquet 2003). Most notably, they have the potential to reveal the specific processes that occur during the lifetime of EC (Chang et al. 2002); such studies, however, require the use of limited-area energy budgets, which differ considerably from their global counterparts.

In limited-area energy budgets emerge additional boundary flux terms that represent energy transferred between the regional and global systems. New perspectives into the study of regional atmospheric energetics have emerged from the work of Orlanski et al. (1991,1993a, 1993b, 1995) who underlined the role of ageostrophic geopotential fluxes in the development of baroclinic waves. Such fluxes cancel out in global energy budgets and hence could not have been identified otherwise.

Since its inception, the derivation of limited-domain energetics has proven itself to be quite challenging. Hence, several studies have rather used a global scheme and defined the energy of a storm as the local contribution to the global budget (Smith 1969; Johnson 1970; Michaelides 1987). This is problematic mainly since such an approach is based on a global reference state (Marquet 1996), but the utilization of a localized budget is considered a sensitive issue (Plumb 1986) "due

54 to the non-uniqueness of the boundary flux and conversion terms [that must be] interpreted with
55 care" (Chang et al. 2002).

56 Many difficulties related to the regional application of Lorenz's approach are solved by redefining
57 an available energy in terms of enthalpy and entropy (Pearce 1978; Marquet 1990). By dividing
58 the available energy into an isobaric temperature-dependent component and a static stability
59 component that accounts for the lapse rate, Marquet (1990) developed an exact local formulation
60 following a classical thermodynamic approach with an energy cycle based on available enthalpy
61 (AE) (Norman 1946), quite similar to that of Pearce's APE. Marquet also redefined the reference
62 state as a spatial and temporal average over large scales. Marquet's derivation then followed
63 closely that of Pearce but for a limited area, therefore requiring additional boundary flux terms for
64 each energy reservoir in order to be complete.

65 Nikiéma and Laprise (2013, hereby NL13) followed a similar approach to that of Marquet in the
66 interest of developing an approximate regional cycle for inter-member (internal) variability (IV)
67 in the study of an ensemble of regional climate model (RCM) simulations. They most notably kept
68 the concept of reference state and the decomposition of AE, but unlike Marquet (1990, 1996, 2003)
69 they considered latent heat release in the generation of AE rather than adding the latent energy of
70 water vapour as part of AE. Clément et al. (2016, hereby CNL16) expanded upon NL13's work
71 by considering time mean and variability for the study of the energetics of a specific extratropical
72 cyclone event.

73 This study aims at furthering the understanding of extratropical cyclone energetics. This work will
74 use the approach of CNL16, but unlike CNL16 who studied the energetics in a fixed, Eulerian
75 reference frame, this work will experiment with a Lagrangian framework following a storm's
76 motion. The objective will be to compare the resulting energetics evaluated in Lagrangian
77 reference framework with their Eulerian counterpart for a specific synoptic-scale EC

78 The Lagrangian approach is in principle optimal as it allows energy diagnostics that exclude
79 regions not related to the storm itself (Michaelides et al. 1999; Pinto and Rocha 2011). Many

algorithms already exist to identify storm tracks such as band-pass filters and feature tracking, but few have ever considered using EKE and AE through a Lagrangian framework (Wing 2009). Vincent and Chang (1975) were amongst the first to attempt a Lagrangian approach: they used contour lines of pressure to evaluate KE located within it. Michaelides et al. (1999) used what they called a "semi-Lagrangian approach" by considering a volume bounded by the 1000 and 100 hPa pressure levels and moving horizontally with the cyclone track. Recently Papritz and Schemm (2013) followed the movements of an idealized baroclinic wave by defining a squared-perimeter around the 100 Jm^{-2} contour lines of KE. The authors of these studies concurred that the magnitude and the role of the different energy conversions are most evidenced using a Lagrangian reference system.

The paper is organized as follows. Sect. 2 will present the methodology of the procedure, including the data used as well as the energetic equations and the Lagrangian computational procedure. Results will be analysed in Sect. 3 by comparing the results of Lagrangian and Eulerian references, as well as evaluating the sensibility of energetic contributions to the size and position of the diagnostic domain. Lastly, Sect. 4 will present the summary and conclusions of the study.

2. Materials and methods

2.1 Mathematical procedure

As mentioned previously, the energetics on a limited-area domain are computed by a series of equations initially developed by NL13 and then modified by CNL16 who developed the cycle based on a temporal decomposition. Following CNL16, atmospheric variables Ψ_t are decomposed in their time-mean state $\langle\Psi\rangle = \frac{1}{\tau}\sum_{t=1}^{\tau}\Psi_t$ and deviations $\Psi_t = \Psi - \langle\Psi\rangle$ (also referred to as transient eddies), so that:

$$\Psi(\phi,\varphi,p,t) = \langle\Psi(\phi,\varphi,p)\rangle + \Psi_t(\phi,\varphi,p,t) \quad (1.1)$$

Where ϕ, φ, p and t represent latitude, longitude, pressure and time, respectively.

The instantaneous values of transient-eddy available enthalpy and kinetic energy are obtained as $a_{TV} \propto T'^2$ and $k_{TV} \propto \vec{V}'^2$, while the climatology of transient eddies is obtained by $A_{TV} \equiv \langle a_{TV} \rangle \propto \langle T'^2 \rangle$ and $K_{TV} \equiv \langle k_{TV} \rangle \propto \left\langle \vec{V}'^2 \right\rangle$ as the variance of atmospheric variable Ψ_t:

$$\frac{1}{\tau}\sum_{t=1}^{\tau} \Psi'(\phi,\varphi,k,t)^2 = \left\langle \Psi'(\phi,\varphi,k,t)^2 \right\rangle \tag{1.2}$$

The use of the lower case and upper case serve to differentiate between instantaneous and climatological values, the former being of most interest in this study.

The current study will focus on the transient-eddy energetics and each energy reservoir and conversion terms will have the subscript 'TV' for time variability as depicted by Fig. 1.

For the study of an individual storm, the evolution of two energy reservoirs is described by the following equations:

$$\frac{\partial a_{TV}}{\partial t} = g_{TV} - c_{TV} + c_A - f_{A_{TV}} - h_{A_{TV}} - j_{a_1} - j_{a_2} \tag{1.3}$$

$$\frac{\partial k_{TV}}{\partial t} = c_{TV} + c_K - d_{TV} - f_{K_{TV}} - h_{K_{TV}} - j_k \tag{1.4}$$

where

$$a_{TV} = \frac{C_p}{2T_r} T'^2$$

corresponds to the available enthalpy due to the time variations of temperature, calculated from the instantaneous deviation from the monthly mean. It is divided by T_r that corresponds to the reference state (Marquet 1990); for the current study, the reference temperature has been approximated to 262 K.

Also

$$k_{TV} = \frac{1}{2}\left(\vec{V}' \cdot \vec{V}'\right)$$

is the kinetic energy associated with time variations of the horizontal wind.

The terms on the RHS of (1.3) are evaluated as:

$$c_A = c_{Ah} + c_{Av}$$

$$c_{Ah} = -\frac{C_p}{T_r} V'T' \cdot \nabla \langle T \rangle$$

$$c_{Av} = -\frac{C_p}{T_r} \omega' T' \frac{\partial \langle T \rangle}{\partial p}$$

$$g_{TV} = l\left(\frac{T'}{T_r} Q'\right),$$

$$c_{TV} = \omega' \alpha'$$

$$f_{a_{TV}} = \nabla \cdot \left(\langle V \rangle a_{TV}\right) + \frac{\partial\left(\langle \omega \rangle a_{TV}\right)}{\partial p}$$

$$h_{a_{TV}} = \frac{C_p}{2T_r}\left[\overline{\nabla}\cdot\overline{\overline{V'T'^2}} + \frac{\partial\overline{\omega'T'^2}}{\partial p}\right] \tag{132}$$

$$j_{a1} = -\frac{c_p T'}{T_r}\vec{\nabla}\mathrm{g}\left\langle\vec{V'}T'\right\rangle - \frac{c_p T'}{T_r}\frac{\partial\langle\omega'T'\rangle}{\partial p} \tag{133}$$

$$j_{a2} = -T'\left(\left\langle\frac{Q}{T}\right\rangle + \frac{\langle Q\rangle}{T}\right) \tag{134}$$

The terms on the RHS of (1.4) are evaluated as:

$$c_{TV} = \omega'\alpha' \tag{136}$$

$$c_K = c_{Kh} + c_{Kv} \tag{137}$$

$$C_{Kh} = -\overline{V'}\cdot\left(\overline{V'}\cdot\overline{\nabla}\right)\left\langle\overline{V}\right\rangle \tag{138}$$

$$C_{Kv} = -\overline{V'}\cdot\left(\omega'\frac{\partial\left\langle\overline{V}\right\rangle}{\partial p}\right) \tag{139}$$

$$d_{TV} = -\overline{V'}\mathrm{g}\overline{F'} \tag{140}$$

$$f_{k_{TV}} = \overline{\nabla}\cdot\left(\left\langle\overline{V}\right\rangle k_{TV}\right) + \frac{\partial\left(\langle\omega\rangle k_{TV}\right)}{\partial p} \tag{141}$$

$$h_{k_{TV}} = \overline{\nabla}\cdot\left(k_{TV} + \Phi'\right)\overline{V'} + \frac{\partial\left(k_{TV} + \Phi'\right)\omega'}{\partial p} \tag{142}$$

$$j_{k1} = -\vec{V}'\left\langle \vec{V}'\mathrm{g}\vec{\nabla}\vec{V}' \right\rangle - \vec{V}'\left\langle \omega' \frac{\partial \vec{V}'}{\partial p} \right\rangle$$

143

144 The transient-eddy available enthalpy a_{TV} receives energy from the mean state by the conversion
145 term c_A which represents the transport of sensible heat by synoptic-scale disturbances. Its intensity
146 is defined by the relationship between the perturbation temperature flux and the perturbation wind
147 against along the mean temperature gradient. The conversion term c_A, when positive, acts as a
148 conversion of time-mean energy for a_{TV} by reducing the mean temperature gradient through shifts
149 in air masses, transporting cold (warm) air equatorward (poleward). The term c_A can also be
150 divided into its horizontal (c_{Ah}) and vertical (c_{Av}) components, which will be useful later on the
151 study. The term g_{TV} is a generation source for a_{TV} associated with diabatic generation of AE by
152 heating mechanisms such as differential radiative heating, the release of latent heat energy, thermal
153 diffusion and convection. The baroclinic conversion term, c_{TV}, when positive, transfers the energy
154 of a_{TV} to k_{TV}, which occurs when warm (cold) air masses ascend (descend) when displaced by
155 baroclinic disturbances. This can be understood as lowering the centre of gravity, and the
156 difference between the initial and final state is the amount of kinetic energy that is produced. The
157 barotropic conversion term, c_K acts against the gradient of momentum by transporting momentum
158 horizontally and vertically. The term d_{TV} acts as a sink for k_{TV} and it represents the dissipation of
159 kinetic energy by friction near the surface and by vertical diffusion (CNL16). The boundary terms,
160 $f_{a_{TV}}$ and $f_{k_{TV}}$, contribute when energy enters or leaves the regional domain. The third-order term,
161 $h_{a_{TV}}$, corresponds to the non-geostrophic fluxes of temperature, which is generally negligible. The
162 term $h_{k_{TV}}$ defines ageostrophic geopotential and kinetic fluxes of k_{TV} in a storm. CNL16 also
163 obtained third-order terms (j_{a_1}, j_{a_2}, j_k) connected to both reservoirs but only j_k is considered to
164 have a non-negligible impact.

2.2 Lagrangian procedure

Within a Eulerian reference, the storm's energetics are computed within a diagnostic domain that remains fixed in time, while a Lagrangian reference is chosen to move with the storm; hence this displacement requires additional considerations for the set of previously described equations in which the time variations of a_{TV} and k_{TV} were expressed as local time derivatives. For a Lagrangian reference, total derivatives need to be used and the equations take the following form:

$$\frac{da_{TV}}{dt} = \frac{\partial a_{TV}}{\partial t} + \vec{V}_{frame} \cdot \nabla a_{TV}$$
$$\frac{dk_{TV}}{dt} = \frac{\partial k_{TV}}{\partial t} + \vec{V}_{frame} \cdot \nabla k_{TV} \quad (171)$$

where $\vec{V}_{frame}$ is the horizontal speed at which the diagnostic domain moves while following the system of interest. The Lagrangian time tendencies $L_E = dE/dt$ of both reservoirs $E \in \{a_{TV}, k_{TV}\}$ as well as the reference scheme $\vec{V}_{frame}$ are computed by using a centred finite-difference method over 6-hourly intervals. In this work the shape and area of the diagnostic domain over which the local time derivatives are computed are kept constant.

During the lifetime of a specific storm, the time tendencies initially grow and then decay; hence integrated over sufficient time intervals and spatial domain, they should vanish. In practice, however, the presence of computational errors, physical approximations, interpolations and the inevitable finite spatial and temporal computational limits prevent obtaining exactly vanishing values, as well as an exact correspondence between the left-hand side tendencies L and the sum of the right-hand side contributions (R). A comparison between L and R remains nonetheless a useful method to evaluate the accuracy of the computed energetics. Spatial derivatives are approximated as centred finite differences and vertical integrals are computed using the trapezoidal rule after eliminating contributions below the surface, as in CNL16.

A Lagrangian diagnostic domain was defined as a rectangle within the CRCM5 computational grid, tracking the selected storm's path. A rectangle was employed to facilitate programming and to preserve a nearly constant surface area during the tracking process, which also eases the interpretation of boundary fluxes. The tracking process was divided into several steps that may be summarized as follows. The tracking rectangle shape and size was selected such that vertically integrated a_{TV} and k_{TV} fields would remain essentially confined within the tracking rectangle. It was noted that simply using k_{TV} was sufficient to shape the reference as it encompassed both a_{TV} and k_{TV}. The motion of the shape was determined as to track the high-energy values of k_{TV} only, and the process was repeated on every diagnostic time. Lagrangian results are then compared to those obtained with a Eulerian framework over a domain size encompassing the region swept by the moving Lagrangian figure.

2.3 Model configuration

Atmospheric variables used to compute the energy cycle originate from a segment of a 35-year-long simulation performed by the 5th generation of the Canadian Regional Climate Model (CRCM5; Martynov et al. 2012; Hernández-Diáz et al. 2012). CRCM5 derives from a limited-area configuration of the global GEM (version 3) used at the Canadian Meteorological Centre (CMC) for the Global Deterministic Prediction System (GPDS) (Côté et al. 1998).

The CRCM5 simulation begins January 1st 1979 at 00 UTC, driven by ERA-Interim (Dee et al. 2011) reanalyses available on a 0.75^{o} grid. The reanalyses serve to prescribe sea surface temperatures (SST) and sea-ice coverage (SIC), as well as the atmospheric lateral boundary conditions (LBC) for each time step after the data has been interpolated in time and space on the RCM grid. In CRCM5 the land-surface conditions are calculated with the Canadian LAnd Surface Scheme (CLASS) v3.5 (Verseghy 2000, 2009) and an interactive column lake module is also included (Martynov et al. 2012). The CRCM5 simulation is configured for a 0.44^{o} rotated latitude and longitude grid mesh, with a free domain of 260 by 160 grid points in the horizontal, covering Canada, USA, Greenland, the north of Mexico, and neighbouring oceans (Fig. 2). The simulation

212 uses 56 terrain-following hybrid levels in the vertical, up to 10 hPa, and the timestep is 12 minutes.
213 Output data is archived at three hourly intervals, interpolated on 19 pressure levels, but energy
214 diagnostics will only be evaluated from 1000 to 150 hPa.

215 The CRCM5-simulated fields rather than the reanalyses fields will be used for the energetic
216 calculations for 2 main reasons: the simulation provides superior time and spatial resolutions, and
217 several fields required by the energy budget are not routinely available in the reanalyses.

218 2.4 Storm selection and synoptic overview

219 In order to facilitate testing the proposed procedure for carrying energy budget calculations in a
220 Lagrangian framework, it was deemed preferable to select a rather mainstream extratropical storm
221 that did not merge or split during its lifetime. A rectangular area was selected that would allow
222 resolving the storm at the various stages of its life cycle within the confinement of the
223 computational domain, which would minimize artefact due to limits imposed by it, as would occur,
224 for instance, if part of the storm were to leave the domain while being tracked. The selected storm
225 has been documented as a significant winter storm due to its heavy precipitation, freezing rain and
226 flooding across the northeastern USA and eastern Canada (NWS 2010). Weather charts for daily
227 values of sea-level pressure, 850 hPa temperature and 500 hPa geopotential height are shown in
228 Fig. 2, from December 09, 00 UTC to December 16, 00 UTC of 2010 (the storm continued until
229 December 18, but the data is not shown). The early stage of the storm can be noted from the 9th of
230 December to 12th of December, with a strong zonal flow across western North America as a result
231 of the Aleutian low pressure south of Alaska and a stationary North Pacific anticyclone. A
232 weakening of the Aleutian low allowed the North Pacific high pressure to shift northward, as seen
233 by an upper level ridge visible from 10-11 December, resulting in the upper level jet acquiring an
234 anticyclonic circulation on the western side of the continent. The equatorward motion of cold air
235 along the upper level trough led to a discernable cyclogenesis by 12th of December. A good
236 indicator of the baroclinic system strengthening is the vertically tilted through, with the axis of the
237 surface pressure center located east of the upper level through. The system reached high intensity
238 by 13th of December when it began to draw moisture from the Gulf Stream and to receive support

239 from the advection of warm air on the eastern side of the low pressure. It moved northeastward
240 along the East Coast, reaching peak intensity on the 14th of December. The vertical tilt then began
241 decreasing and the storm weakened. The occluded phase becomes evident when the upper level
242 trough closed around December 16, 00 UTC, hence shutting off the upper level support. The
243 system's only remaining support arose from the warm air advection to the north of its centre. After
244 16th December, the system moved slightly westward and the warm front eventually detached itself
245 from the remnants of the storm, which quickly dissipated afterwards. The study of the storm halts
246 at December 18, 00 UTC because most of the storm's energy reached negligible values.

247 Fig. 3 shows a time series of minimum sea level pressure during the month of December 2010,
248 along with spatial mean and vertically integrated values of a_{TV} and k_{TV} on the entire domain. The
249 strength of the storm and duration of the EC is well illustrated as the lowest values of sea level
250 pressure simultaneous occur at the same time of a peak in k_{TV} between December 10-18th as shown
251 in Fig. 3. It is noteworthy, however, that a_{TV} exhibits little time variation; the choice of the
252 diagnostic domain can affect the results, as will also be evaluated later.

253 2.5 Analytical tools

254 From the CRCM5 model outputs, the energetic equations were computed using a set of utilities
255 (r.diag, graciously maintained by Dr. Bernard Dugas) through Linux Shell scripting. Once each
256 energetic term has been computed, the application of the Lagrangian framework on the terms was
257 designed and executed using the MATLAB software (version 2017b, MATLAB 2017); this
258 software was also employed to plot results.

259

260

261

3. Results and discussion

3.1 Comparison of eddy energy reservoirs

3.1.1 Time series and vertical profiles

The interest of employing a Lagrangian reference framework for computing energetics becomes apparent in Fig. 4 and 5 that compare the energetics using Lagrangian and Eulerian frameworks. Fig. 4a shows time series of domain-integrated values of transient-eddy kinetic energy (k_{TV}) and available enthalpy (a_{TV}) reservoirs, for the Lagrangian and Eulerian frameworks. The storm increased in intensity from 10th to the 14th of December and decreased during the following four days. There is a considerable difference in the calculated storm intensity between the results obtained with the two frameworks, the strongest values being obtained with the Lagrangian one. This is consistent with previously cited atmospheric energetics studies using a similar methodology (Vincent and Chang 1975; Michealides et al. 1999; Papritz and Schemm 2013). Fig. 4b shows a time series of energy tendencies. The k_{TV} tendency computed with the Lagrangian framework clearly depicts the periods at which the system grows and decays, while this is far less obvious with the Eulerian one. The amplitude is larger and provides a higher realistic understanding of how the storm evolves through time. When comparing the time-mean tendencies, the Lagrangian framework gives $L_{a_{TV}} = 0.46\ J\ m^{-2}$ and $L_{k_{TV}} = 0.52\ J\ m^{-2}$, while the Eulerian framework gives $L_{a_{TV}} = 0.20\ J\ m^{-2}$ and $L_{k_{TV}} = 0.28\ J\ m^{-2}$. These values are fairly small compared to the instantaneous values of tendencies, hence indicating a fairly closed system.

Fig. 5 shows a vertical profile of time-averaged energetics between 13-15 December, corresponding to the peak intensity period. The figure compares horizontally and vertically integrated a_{TV} and k_{TV} for the Lagrangian and Eulerian intensity. It can be seen that k_{TV} is strongest in the upper troposphere near the location of the jet stream. The vertical profile of a_{TV} shows nearly uniform values below 400 hPa, where maximum temperature advection occurs. In both cases, the Lagrangian intensity energetics are systematically stronger.

3.1.2 Map of energy reservoirs

Fig. 6 shows maps of the spatial structure of the vertically integrated values of a_{TV} and k_{TV} during the evolution of the weather system. As is to be expected, peak values of a_{TV} are located in areas where there are significant temperature anomalies (panel in Fig. 6a). These anomalies can be more easily understood when comparing the panels Fig 6 with the 850 hPa temperature maps of the panels in Fig 2. There are noticeable alignments between the areas of intense a_{TV} around the low-pressure center (panel Fig. 6a) with the areas consisting of cold and warm air advection. Near 14, 00 UTC, two peaks of a_{TV} are noticeable, associated with the warm and cold sectors of the storm. Later the warm air advection dominates as the storm occludes and moves northwestward. The spatial pattern of k_{TV} shown in Fig. 6b closely reflects the jet stream (not shown) and it is initially strongest to the west of the trough. The initial peak of k_{TV} is located west of the developing low-pressure centre, and it later shifts towards its centre by 13, 00 UTC. Up until the dissipation phase, the energy east of the trough is included within the storm's energy, but as the trough expands near the end of the storm's life, the energy located over it no longer becomes relevant.

3.2 Comparison of energetic contributions

3.2.1 Time series and vertical profiles

Fig. 7 displays the times series for the various contributions to the domain-averaged a_{TV} (Fig 7a) and k_{TV} (Fig 7b) tendencies, and Fig. 8 presents the vertical profiles of these contributions. Results indicate stronger magnitude for the energy evaluated under the Lagrangian framework than the Eulerian one for every contribution. When looking at each contribution individually, the Eulerian results are similar to that of CNL16 and Nikiéma et al. (2017). For example, the approximate duality in magnitude and pattern between c_{TV} and c_A is noteworthy in Fig. 7a. As seen in Fig. 8a, there is also an important contribution of g_{TV} that peaks in the mid-troposphere, where clouds and precipitation form in extratropical cyclones, reflecting the release of latent heat energy. This would hence corroborate the findings of previous work that noted that latent heat release is a strong

312 component of transient-eddy energy generation for mid-latitude cyclones (Danard 1966; Bullock
313 and Johnson 1971; Michaelides 1987). A negative product between Q' and T' can lead to negative
314 values of g_{TV} which occur near the surface (Fig. 8a). This is due to boundary-layer heat flux that
315 is frequently occurs during winter (Nikiéma et al. 2017). During the second period, the contribution
316 of g_{TV} slightly extends downwards to 800 hPa and has greater negative magnitude near the surface.

317 There are also notable differences when comparing the baroclinic conversion terms. In both
318 periods, there are asymmetrical distributions of c_{TV} and c_A, with c_{TV} being larger at higher levels
319 in both instances; this may be expected as c_A represents the horizontal distribution of air masses,
320 while c_{TV} is their corresponding rising and sinking motions. The distribution shifts towards the
321 lower levels in decaying phase with c_A reaching peak values between 700-800 hPa and c_{TV}
322 between 500-700 hPa.

323 The energetic contributions to k_{TV} are shown in Fig. 7b and Fig. 8b. High values of energy
324 dissipation d_{TV} are directly associated with the intensity of the wind perturbations, which explains
325 why it is strongest when the storm reaches full maturity near December 14, 00 UTC. It is also
326 strongest near the surface, as indicated by the vertical profiles due to surface friction, and its
327 magnitude decreases with height. The barotropic contribution c_K becomes negative and with
328 greater magnitude in the decaying phase of the storm, as shown within Fig. 7b, indicating a
329 conversion of kinetic energy from the storm to the mean flow. This occurs when the storm occludes
330 and enters a barotropic state. Fig. 8b also reveals that c_K is largest near the tropopause where the
331 jet stream is located.

332 The term $h_{k_{TV}}$ acts as the main energy sink throughout the entire storm, except between 10-12
333 December when it acts as a source. This positive maximum of $h_{k_{TV}}$ precedes the baroclinic
334 conversion and could consequently represent the ageostrophic convergence of energy, which
335 might act as an initial amplifier for the disturbance, as noted by Orlanski and Sheldon (1995). Their

study showed ageostrophic geopotential flux convergence of downstream development that occurs in the upper troposphere and is intrinsically linked with energy transfers between consecutive cyclones, the study of which however is beyond the scope of this work. Most importantly, one must note that these early positive values of $h_{k_{TV}}$ are not seen with the Eulerian framework. The vertical distribution of $h_{k_{TV}}$ in Fig. 8b shows negative values within the boundary layer that acts as a source. It physically represents the Ekman pumping that counterbalances the frictional loss d_{TV} (Nikiema and Laprise 2015; Nikiéma et al. 2017). It is a source of energy for the storm because of low-level convergence induced by non-geostrophic winds, whose intensity is related to surface friction. There is also a significant increase in $h_{k_{TV}}$ throughout the middle and higher levels in the last four days of the storm. These values are problematic since it leads to a net negative energetic budget. Additional insight on this behaviour can be obtained by looking at its spatial distribution. Another component of $h_{k_{TV}}$ has been noted in a study done by Rivière and Arbogast (2015) who noted a downward redistribution of eddy kinetic energy by vertical ageostrophic flux during the later stages of large-scale cyclones. Such redistribution, however, has not been observed in this EC (not shown).

Lastly, values of $h_{a_{TV}}$ are negligible, and likewise for $f_{a_{TV}}$ and $f_{k_{TV}}$. These last two terms only acquire non-negligible values when high values of energy develop within the domain. The advection of a_{TV} is negligible throughout the period, while the advection of k_{TV} is significant in the later phase. Its pattern, illustrated in Fig. 6b, resembles closely to that of $h_{k_{TV}}$. It is also strongest in the higher levels as shown by Fig. 8b. This behaviour can somewhat be explained when looking at the mathematical expression of $V_{frame}\mathrm{g}\nabla k_{TV}$ and $h_{k_{TV}}$, where both terms contain the horizontal gradient of k_{TV}.

3.2.2 Maps of contributions to the energy tendencies

Fig. 9 shows the most important contributions to both energy reservoirs. Conversion term c_A characterizes the energy associated with horizontal and vertical transport of temperature along the mean horizontal and vertical gradients of temperature. Near the surface, positive values $v'T' > 0$ are initially seen west of the storm, where there is southward advection of cold air, followed later by a northward advection of warm air east of the storm. It is however the vertical component of c_A that dominates, as illustrated in Fig. 10, and its shape closely resembles that of c_{TV}. In the case of c_{TV}, interpreted as a sinking ($\omega' > 0$) of colder air ($T' < 0$) or a rising ($\omega' < 0$) of warmer air ($T' > 0$), both leading to negative conversion values ($\omega'T' < 0$) making it act as a sink for a_{TV}, while the vertical component of c_A acts as a source, hence the noted near duality.

When evaluating c_K, slight dipoles are noticeable near the low-pressure centre during the early stages of the storm, but with positive values dominating, leading to a source for k_{TV}. It only begins acting as a sink on 14, 00 UTC. Fig. 11 shows that the rate of conversion for the sink is amplified by the positive product of u' and v', and strong positive values of $\partial\langle u\rangle/\partial\Phi$ (note the negative sign of the equation in section 2.1) representing the wind shear induced by the jet stream. In all occurrences, the horizontal transfer is stronger than the vertical one, supporting the results of van Mieghem (1955). This explains why this conversion term is known as barotropic, because even in the absence of baroclinicity, c_K remains strong.

The term $h_{k_{TV}}$ is shown (Fig. 8d) to have the strongest and most chaotic values of all the terms. It is noteworthy to add at this point that the interval scale is logarithmic, consequently making the spatial distribution of $h_{k_{TV}}$ towering over all the others. Numerous dipoles are noticeable around the storm and within the diagnostic rectangular, with negative values over the low-pressure centre from 13, 00 UTC to 15, 00 UTC, and positive values surrounding it. Near the end of the cycle, the dipole remains present, but the positive component is left out of the Lagrangian domain, leaving

384 consequently a widespread amount of negative values within it. This could indicate that, unlike
385 every other components of the cycle, the boundary term $h_{k_{TV}}$ related the storm are not as clearly
386 defined and possibly more widespread, thus making it difficult to evaluate adequately.

387 3.3 Comparison of energy cycle and budget equilibrium

388 Fig. 12 shows the space-time mean of the components to the transient-eddy energy budget of the
389 studied storm from December 10, 0000 UTC to December 18, 0000 UTC. The sum of the terms
390 contributing to transient-eddy available enthalpy a_{TV} is fairly small, $R - Lag_{a_{TV}} = 0.17$ W m^{-2} and
391 $R - Eul_{a_{TV}} = -0.29$ W m^{-2}, indicating a fairly closed a_{TV} budget considering that the individual
392 contributions to the tendencies are of the order of 1 to 10 W m^{-2}, and that the time-mean tendencies
393 are $L_{a_{TV}} = 0.46$ W m^{-2} and $L_{a_{TV}} = 0.20$ W m^{-2} for the Lagrangian and Eulerian frameworks,
394 respectively. Some significant discrepancy however occurs for the transient-eddy kinetic energy
395 k_{TV} budget, with $R - Lag_{k_{TV}} = -11.66$ W m^{-2} for the Lagrangian framework and
396 $R - Eul_{k_{TV}} = -4.27$ W m^{-2} for the Eulerian one, with the time-mean tendencies $L_{k_{TV}} = 0.52$ W m^{-2}
397 for the Lagrangian framework and $L_{k_{TV}} = 0.28$ W m^{-2} for the Eulerian one. Thus, the large values
398 for the $R - k_{TV}$, notably for the Lagrangian framework, requires consideration.

399 The impact of the size of the Lagrangian diagnostic domain on the energy budget was tested, as
400 shown in Fig. 13. The horizontal axis shows the number of grid points removed or added to the
401 previously used rectangle, while the four lines correspond to the four cardinal directions. There
402 are modest changes in variations for a_{TV}, the largest ones occurring in the +X and +Y directions
403 where magnitude of the departure increases when the size of the diagnostic domain is reduced in
404 the +Y or increased in the +X directions. In the case of k_{TV}, however, significant changes in values
405 occur linearly in the +X and -X directions, with shrinking large values. The changes in budget
406 values in the + and –Y directions are minor. Such sensitivity study gives a sense of the stability of

407 the overall budget values. Although not shown, the shifts in location revealed similar results to
408 that of modifications in the size.

409 It is then relevant to determine how individual components of the budget change as a function of
410 the Lagrangian diagnostic domain size. As noted previously, the large negative values of $h_{k_{TV}}$
411 contribute to the overall negative tendency in the last three days of the storm (Fig. 9d). The effect
412 of increasing the Lagrangian diagnostic domain size in the four horizontal directions is shown in
413 Fig. 14 and Fig. 15 for each individual component, during 17 December 00 UTC. Fig. 14 only
414 shows the modifications for $h_{k_{TV}}$ with the horizontal axis showing the number of grid points added,
415 while the four lines correspond to the four cardinal directions. Each line stops when the diagnostic
416 domain reaches the CRCM5 computational domain boundary or when it extended by 60 grid points.
417 It is apparent that smaller values of $h_{k_{TV}}$ are obtained when the domain is extended in the -X and -
418 Y directions; minimum values are reached when the -X direction is extended by 25-30 grid points
419 and more than 60 grid points for the -Y direction. Fig. 15 displays changes in the various
420 contributions when the diagnostic domain is changed in either the -X or the -Y directions. In all
421 figures, most terms show little variations in the energetic values. There are some noticeable
422 variations in c_A and c_{TV}, in both directions, but proportionally less than that of $h_{k_{TV}}$. These results
423 lead to conclude that the current shape and position of the diagnostic Lagrangian domain is close
424 to being optimal given that extending in +X and +Y would rapidly increase the contribution values,
425 while going in -X or -Y would take a significant number of grid points to produce significant
426 decreases; the configuration would no longer follow closely the storm of interest. Likewise,
427 applying minor changes in size or position of the reference during the storm's life span would not
428 have a significant impact on the overall budget.

429 It appears that the large negative values of $h_{k_{TV}}$ exist because there are no compensating positive
430 values within the retained diagnostic domain. Indeed, when inspecting other moments in the
431 storm's life and the results obtained by CNL16 and Nikiéma et al. (2017), there is always a
432 noticeable duality between negative and positive values for $h_{k_{TV}}$. Even when evaluating the

433 Eulerian budget (Fig. 12), $R - Eul_{k_{TV}}$ is fairly high due to high values of $h_{k_{TV}}$ near the end of the
434 cyclone's life. In this case, it is most likely because a portion of positive $h_{k_{TV}}$ energy is out of the
435 Lagrangian diagnostic domain at the northeastern boundary (Fig. 9d).

436 4. Summary and conclusion

437 The purpose of this work was to compare regional atmospheric energy budget for an EC occurring
438 over North America under two different perspectives: a Eulerian framework where budget
439 diagnostics are computed over a wide and fixed domain, and a Lagrangian framework where these
440 computations are performed over a smaller but mobile domain that tracks the system through its
441 eddy kinetic energy. A hypothesis was put forward that the latter method is the optimal approach
442 to adequately interpret an EC because the analysis would most notably reveal stronger energetics
443 as well as otherwise concealed properties as would be the case under a Eulerian framework.

444 The energy budget was established by decomposing atmospheric variables in their time-mean state
445 and time variability. For the study of individual systems, the time variability is the only relevant
446 component. With a simulation performed by the CRCM5 over a 0.44^{o} grid mesh and driven by
447 ERA-Interim reanalyses, an extratropical cyclone occurring between December 10-18th 2010 was
448 chosen to test the methodology. As this is a recently developed approach, the EC was chosen so
449 that it did not display any behaviour that differs substantially from a typical textbook cyclone while
450 also remaining within the confinement of the lateral boundary domain in order to accurately
451 interpret the entire cycle.

452 The employed tracking method defined a rectangular shape frame over a specified threshold of
453 vertically integrated eddy kinetic energy at a specific time in the cyclone's life. Previous and
454 subsequent time steps of the cyclone then received the formerly defined shape based on which
455 high levels of eddy kinetic had the closest resemblance to the eddy kinetic energy of the
456 neighbouring time step. This allowed for a smooth connection between each step all while making
457 use of a simple but effective method.

Previously shown results reveal that when performing a time series of the spatial and vertical mean of each energetic component, the Lagrangian framework confirms the hypothesis as each component demonstrates stronger amplitude compared to the fixed framework. Most importantly, evaluating the time series of the temporal tendencies under the moving domain remarkably reveals a clear distinction between the increasing and decreasing phases of energetic strength of the EC while this is difficult to adequately distinguish within the fixed domain. This clear distinction enables a separation between these two periods with the increasing stage occurring between December 10-14th and the decreasing phase occurring between December 14-18th. Subsequently, a vertical interpretation of each component separated in these two periods exposed noticeable differences, most particularly with the baroclinic conversion terms c_A, c_{TV} and the boundary term $h_{k_{TV}}$. It can be noted that the amplitudes of c_A and c_{TV} vertically shift from the upper troposphere to the mid-level and that $h_{k_{TV}}$ becomes considerably negative between the mid and upper troposphere. This consequently leads to an overall negative $R_{k_{TV}}$ and this negative value is far larger for the Lagrangian framework than the Eulerian one. The values of $R_{a_{TV}}$ and the temporal tendencies for a_{TV} and k_{TV} all tend to vanish and the differences between both methods are small. This leads to conclude that the spatial extent at which $h_{k_{TV}}$ has an influence on the EC goes beyond to that of the other components of the cycle. A larger diagnostic domain would be required to encompass this term in its entirety. However, it is also possible that positive values which should counter-balance the observed negative dominance extend beyond the model boundaries. Lastly, the sensitivity of the diagnostic domain to its size and positioning was also evaluated and the results indicate that only $h_{k_{TV}}$ is susceptible to large changes in its computed values.

Ultimately, the Lagrangian framework fulfils its purpose by providing a realistic and accurate depiction of the extratropical cyclone. Through an energy budget, the multiple aspects of a storm are reduced to a common denominator and their aspects are more effectively understood. Many studies have limited themselves with using a fixed and large domain to evaluate its energetic behaviour. Although useful enough to understand the underlying principles of how a storm evolves,

this type of reference lacks the precision that a Lagrangian framework can provide, as was illustrated in this study. As this is a seldom-used method in the study of atmospheric energetics, its potential and the amount of information that can be exploited from it are considerable. Even though this study focused on a synoptic-scale system, this kind of framework can prove itself to be particularly useful for tropical cyclones or mesoscale convective systems. Further use of this method could be found as an automatic storm-tracking algorithm. With the increasing interest in machine learning, a supervised machine-learning algorithm could be devised to distinguish and connect the areas with high a_{TV} and k_{TV} over multiple time steps and devise a tracking system from these formed connections. Another useful way of exploiting this method is through the tracking of a large ensemble of storms and computing various statistical parameters from their compiled energetic values. This type of study could then be extended into a comparison between the energy cycle of storms in the current climate versus that of a changed climate under different emission scenarios. However, and like all storm-tracking methods, this method has limitations in the sense that certain parameters are subjectively based. The prime example of this would be the imposed threshold that distinguishes areas of high energetic values to the low ones. It would be possible for certain systems to exist without ever going pass this threshold value, making them unnoticeable to the algorithm. This problematic would be but one among many others that would need to be considered if such a scientific endeavour were to ever occur.

References

Boer GJ and Lambert S (2008) The energy cycle in atmospheric models. Clim Dyn 30:371-390 doi:10.1007/s00382-007-0303-4

Bullock BR, Johnson DR (1971) The generation of Available Potential Energy by Latent Heat Release in a Mid-Latitude Cyclone. Mon Wea Rev 99:1-14 https://doi.org/10.1175/1520-0493(1971)099<0001:TGOAPE>2.3.CO;2

Chang EK, Lee S, Swanson KL (2002) Storm track dynamics. J Clim 15:2163-2183. doi: 10.1175/1520-0442(2002)015<02163:STD>2.0.CO;2

Clément M, Nikiéma O, Laprise R (2016) Limited-area atmospheric energetics: illustration on a simulation of the CRCM5 over eastern North America for December 2004. Clim Dyn 48:2797-2818 doi:10.1007/s00382-016-3198-0

Côté J, Gravel S, Méthot A, Patoine A, Roch M, Staniforth A (1998) The operational CMC-MRB global environmental multiscale (GEM) model. Part I: design considerations and formulation. Mon Wea Rev 126:1373–1395. doi: 10.1175/1520-0493(1998)126<1373:TOCMGE>2.0.CO;2

Danard MB (1966) On the Contribution of Released Latent Heat to Changes in Available Potential Energy. J Appl Meteorol 5:81–84, https://doi.org/10.1175/1520-0450(1966)005<0081:OTCORL>2.0.CO;2

Dee DP, Uppala SM, Simmons AJ, Berrisford P, Poli P, Kobayashi S, Andrae U, Balmaseda MA, Balsamo G, Bauer P (2011) The ERA-Interim reanalysis: configuration and performance of the data assimilation system. Q J Royal Meteorol Soc 137:553–597. doi:10.1002/qj.828

Dutton JA, Johnson DR (1967) The theory of available potential energy and a variational approach to atmospheric energetics. Adv Geophys 12:107-111. doi: 10.1016/S0065-2687(08)60379-9

Fjortoft (1951) The stability properties of large-scale atmospheric disturbances. Am Meteorol Soc 454-463. DOI: https://doi.org/10.1007/978-1-940033-70-9_38

Hernández-Díaz L, Laprise R, Sushama L, Martynov A, Winger K and Dugas B (2012) Climate simulation over CORDEX Africa domain using the fifth-generation Canadian

Regional Climate Model (CRCM5). Clim Dyn 40(5-6):1415-1433 doi:10.1007/s00382-012-1387-z

Johnson DR (1970) The available potential energy in storms. J Atmos Sci 27:727–741 doi:10.1175/1520-0469(1970)027<0727:TAPEOS>2.0.CO;2

Kuo HL (1951) A note on the kinetic energy balance of the zonal wind systems. Tellus 3:205-207

Lorenz EN (1955) Available potential energy and the maintenance of the general circulation. Tellus 7:157-167

Lorenz EN (1967) The nature and theory of the general circulation of the atmosphere. World Meteorol Organ 218 TP 115 pp 161

MATLAB (2017b) The MathWorks, Inc., Natick, Massachusetts, United States.

Margules M (1905) Über die Energie der Stürme. In: Jahrbuch der Kaiserlich-Königliche Zentralanstalt für Meteorologie und Erdmagnetismus in Wien, NF, Bd. 42

Marquet P (1990) On the concept of available enthalpy: Application to atmospheric energetics. C R Acad Sci 310: 1387-1392

Marquet P (1996) L'énergie utilisable de l'atmosphère. La Météorologie. 8^{e} série 14:11-26

Marquet P (2003) The available-enthalpy cycle. I: Introduction and basic equations. Q J R Meteorol Soc 129 :2445-2466. doi:10.1256/qj.01.62

Martynov A, Sushama L, Laprise R, Winger K, Dugas B (2012) Interactive lakes in the Canadian Regional Climate Model, version 5: the role of lakes in the regional climate of North America. Tellus Ser A 64:16226, doi: 10.3402/tellusa.v6i0.16226

Michaelides SC (1987) Limited Area Energetics of Genoa Cyclogenesis. Mon Wea Rev 115:13–26. https://doi.org/10.1175/1520-0493(1987)115<0013:LAEOGC>2.0.CO;2

Michaelides S, Prezerakos NG, Flocas HA (1999) Quasi-Lagrangian energetics of an intense Mediterranean cyclone. Q J R Meteorol Soc 125(553):139-168.

Muench HS (1965) On the dynamics of the wintertime stratosphere circulation. J Atmos Sci 22:349-360. https://doi.org/10.1175/1520-0469(1965)022<0349:OTDOTW>2.0.CO;2

Nikiéma O, Laprise R (2013) An approximate energy cycle for inter-member variability in ensemble simulations of a regional climate model. Clim Dyn 44(3–4):831–852. doi:10.1007/s00382-012-1575-x

Nikiéma O, Laprise R (2015) Energy cycle associated with inter-mem- ber variability in a large ensemble of simulations with the Cana- dian RCM (CRCM5). Clim Dyn. doi:10.1007/s00382-015-2604-3

Nikiéma O, Laprise R, Dugas B (2017) Energetics of transient-eddy and inter-member variabilities in global and regional climate model simulations. Clim Dyn 44(3–4):831–852. doi:10.1007/s00382-017-3918-0

Norman SC (1946) Energy in the atmosphere. Q J R Meteorol Soc 72:145-167

NWS (2010) The Blizzard and Winter Storm of December 11-12, 2010. Available from https://www.weather.gov/grb/121210_blizzard. Last consulted Septembre 13th, 2020.

O'Gorman PA, Schneider T (2008) Energy of Midlatitude Transient Eddies in Idealized Simulations of Changed Climates. J Clim 21:5797–5806. https://doi.org/10.1175/2008JCLI2099.1

Orlanski I, Katzfey J (1991) The Life Cycle of a Cyclone Wave in the Southern Hemisphere. Part I: Eddy Energy Budget. J Atmos Sci 48:1972–1998. https://doi.org/10.1175/1520-0469(1991)048<1972:TLCOAC>2.0.CO;2

Orlanski I, Chang EK (1993a) Ageostrophic Geopotential Fluxes in Downstream and Upstream Development of Baroclinic Waves. J Atmos Sci 50:212–225. https://doi.org/10.1175/1520-0469(1993)050<0212:AGFIDA>2.0.CO;2

Orlanski I, Sheldon J (1993b) A Case of Downstream Baroclinic Development over Western North America. Mon Wea Rev 121:2929–2950. https://doi.org/10.1175/1520-0493(1993)121<2929:ACODBD>2.0.CO;2

Orlanski I, Sheldon J (1995) Stages in the energetics of baroclinic systems. Tellus A 47:605-628. doi:10.1034/j.1600-0870.1995.00108.x

Oort AH (1964) On estimates of the atmospheric energy cycle. Mon Wea Rev 92:483-493. https://doi.org/10.1175/1520-0493(1964)092<0483:OEOTAE>2.3.CO;2

Papritz L, Schemm S (2013) Development of an idealised downstream cyclone: Eulerian and Lagrangian perspective on the kinetic energy. Tellus 65:19539. doi: 10.3402/tellusa.v65i0.19539

Pearce RP (1978) On the concept of available potential energy. Q J R Meteorol Soc 104:737-755

Peixoto JP, Oort AH (1974) The Annual Distribution of Atmospheric Energy on a Planetary Scale. J Geophys Res 20:2149-2159. https://doi.org/10.1029/JC079i015p02149

Pinto JRD, Rocha RPD (2011). The energy cycle and structural evolution of cyclones over southeastern South America in three case studies. J Geophys Res 116 doi: 10.1029/2011JD016217

Plumb RA (1986) Three-Dimensional Propagation of Transient Quasi-Geostrophic Eddies and Its Relationship with the Eddy Forcing of the Time—Mean Flow. J Atmos Sci 43:1657–1678, https://doi.org/10.1175/1520-0469(1986)043<1657:TDPOTQ>2.0.CO;2

Rivière, G, Arbogast P (2015). Eddy kinetic-energy redistribution within idealized extratropical cyclones using a two-layer quasi-geostrophic model. Q J R Meteorolol Soc 141:10. DOI: 10.1002/qj.2350

Smith PJ (1969) On the contribution of a limited region to the global energy budget. Tellus 21:202–207. doi:10.1111/j.2153-3490.1969.tb00432.x

Starr VP, White RM (1951) A hemispherical study of the atmospheric angular-momentum balance. Q J R Meteorol Soc 77: 215-225. doi:10.1002/qj.49707733206

Starr VP (1953) Note Concerning the Nature of the Large-Scale Eddies in the Atmosphere. Tellus 5,4: 494-498. DOI: 10.3402/tellusa.v5i4.8694

Starr VP (1954) Commentaries Concerning Research on the General Circulation. Tellus 6:268–27

Tamura S (1905) Doctor Margules on the energy of storms. Mon Weather Rev 33:519–521

Ulbrich U, Speth R (1991) The Global Energy Cycle of Stationary and Transient Atmospheric Waves: Results from ECMWF Analyses. Meteorol Atmos Phys 45:125–131

van Mieghem J (1952) Energy conversions in the atmosphere on the scale of the general circulation. Tellus 4:334-351. doi:10.1111/j.2153-3490.1952.tb01022.x

van Mieghem J (1955) Note on the energy transfer and conversion in large atmospheric disturbances. Q J R Meteor Soc 81:19-22

van Mieghem J (1959) On the Selective role of the motion systems in the atmospheric general circulation. The atmosphere and the sea in motion. 230-239 (222)

Verseghy D (2000) The Canadian land surface scheme (CLASS): its history and future. Atmos Ocean 38:1–13. doi: 10.1080/07055900.2000.9649637

Verseghy D (2009) The Canadian land surface scheme: technical documentation—version 3.4. Climate Research Division, Science and Technology Branch, Environment Canada. pp 183

Vincent DG, Chang LN (1975) Kinetic energy budgets of moving systems: Case studies for an extratropical cyclone and hurricane Celia, 1970. Tellus 27:215-233. doi:10.1111/j.2153-3490.1975.tb01674.x

Wiin-Nielsen, A. On the annual variation and spectral distribution of atmospheric energy. Tellus 19, 540–559 (1967)

Wing A (2009) Storm track review. Florida State University. pp 24

Yeong KH, Maeng KK (2013) Examination of the global Lorenz energy cycle using MERRA and NCEP-reanalysis 2. Clim Dyn. 40:1499-1513. doi:10.1007/s00382-012-1358-4

List of figure legends

Fig. 1 Limited-area energy cycle for transient eddies, following the methodology developed by NL13 and applied for temporal disturbances by CNL16.

Fig. 2 Instantaneous maps of 850-hPa temperature (in colour), with 500-hPa geopotential height (in red contours) and mean sea level pressure (in black contours), from 09 to 16 December 2010, all at 00 UTC. Units: temperature (°C), sea level pressure (hPa), geopotential height (dam). Images are rotated -90 degrees.

Fig. 3 Time series through the month of December 2010 of vertically integrated (1000-150 hPa) and spatial averaged transient-eddy available enthalpy (a_{TV}, red line) and kinetic energy (k_{TV}, blue line), as well as minimum mean sea level pressure (black line) over the entire domain. The shaded area covers the period of December 10-18th, when the storm occurred.

Fig. 4 Time evolution between December 10-18 of vertically integrated (1000-150 hPa) and spatial averaged transient-eddy reservoirs (k_{TV} and a_{TV}) for Lagrangian (full lines) and Eulerian (dotted lines) reference frames.

Fig. 5 Vertical profile of spatially and temporally averaged over the period of December 13 to 15th of transient-eddy reservoirs (a_{TV} and k_{TV}), for Lagrangian (full lines) and Eulerian (dotted lines) reference frames.

Fig. 6 Maps of vertically integrated transient-eddy energy reservoirs a_{tv} (a) and k_{tv} (b) in colour (10^5 J m^{-2}), for the period from 12 to 17 December 2010. The black rectangle shows the location of the Lagrangian diagnostic domain, while the red rectangle shows the Eulerian diagnostic domain. Black contours show mean sea level pressure (hPa).

Fig. 7 Time series of the contributions to the tendency of transient-eddy available enthalpy a_{tv} (a) and kinetic energy k_{tv} (b). The sign of each contribution reflects whether it is a sink (<0) or a source (>0) to its corresponding reservoir

Fig. 8 Vertical profiles of the contributions to the tendency of a_{TV} (a) and k_{TV} (b) in the Lagrangian (full lines) and Eulerian (dotted lines) reference frames, averaged between December 10-14th (the growing period; left-hand side) and December 14-18th (the decaying period; right-hand side).

Fig. 9 Maps of vertically integrated contributions to energy tendencies: c_A (a), c_{TV} (b), c_K (c), $-h_{k_{TV}}$ (d). The black rectangle shows the location of the Lagrangian diagnostic domain, while the red rectangle shows the Eulerian diagnostic domain.

Fig. 10 Time sequence of vertically integrated and spatially averaged value of the conversion term c_A in the Lagrangian reference frame, and its decomposition in its vertical (c_{Av}) and horizontal components (c_{Ah}). The horizontal component is further divided into longitude-oriented (c_{Ah1}) and latitude-oriented (c_{Ah2}) parts such that $c_{Ah} = c_{Ah1} + c_{Ah2}$. The sign of each contribution reflects whether it is a sink (<0) or a source (>0) to the a_{tv} reservoir.

Fig. 11 Time sequence of vertically integrated and spatially averaged value of the conversion term c_K in the Lagrangian reference frame, and its decomposition in its vertical (c_{Kv}) and horizontal components (c_{Kh}). The horizontal component is further divided into a variance of zonal and meridional wind of longitude-oriented (c_{Kh1}) and latitude-oriented (c_{Kh2}), as well as a covariance of the pair in a longitude-oriented (c_{Kh3}) and a latitude-oriented (c_{Kh4}) parts. As for the vertical component, it is further divided into the longitude-oriented (c_{Kv1}) and latitude-oriented (c_{Kv2}) parts. The sign of each contribution reflects whether it acts as a sink (<0) or a source (>0) to the k_{TV} reservoir.

Fig. 12 Transient-eddy energy cycle obtained with the Lagrangian reference frame (values in green, above) and the Eulerian reference frame (values in brown, below). Values for the energy contributions and reservoirs have been vertically integrated (1000 – 150 hPa), spatially average over their corresponding Lagrangian or Eulerian diagnostic domains and temporarily averaged between December 10 at 0000 UTC to December 18 at 0000 UTC. Note that the Eulerian reference does not have any advective contribution. Units for the energy contributions and reservoirs are in Wm^{-2} and Jm^{-2}, respectively.

Fig. 13 Energy budget for a_{TV} (a) and k_{TV} (b) when extending or decreasing the Lagrangian diagnostic domain size.

Fig. 14 Variation of the vertically integrated contribution $h_{k_{TV}}$ when extending or decreasing the Lagrangian diagnostic domain size in the four cardinal directions.

Fig. 15 Variation of the vertically integrated contributions to a_{TV} (a and b) and k_{TV} (c and d) when decreasing the Lagrangian diagnostic domain size in -X (a and c) and -Y (b and d) directions.

Figures

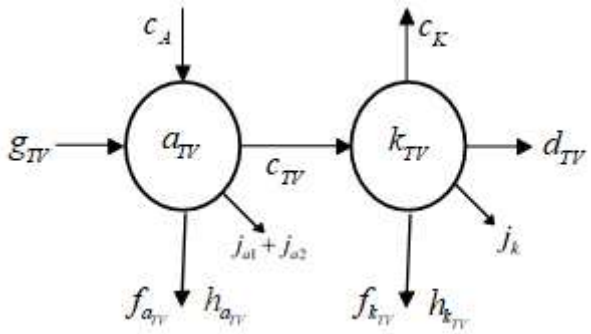

Figure 1

See the Manuscript Files section for the complete figure caption.

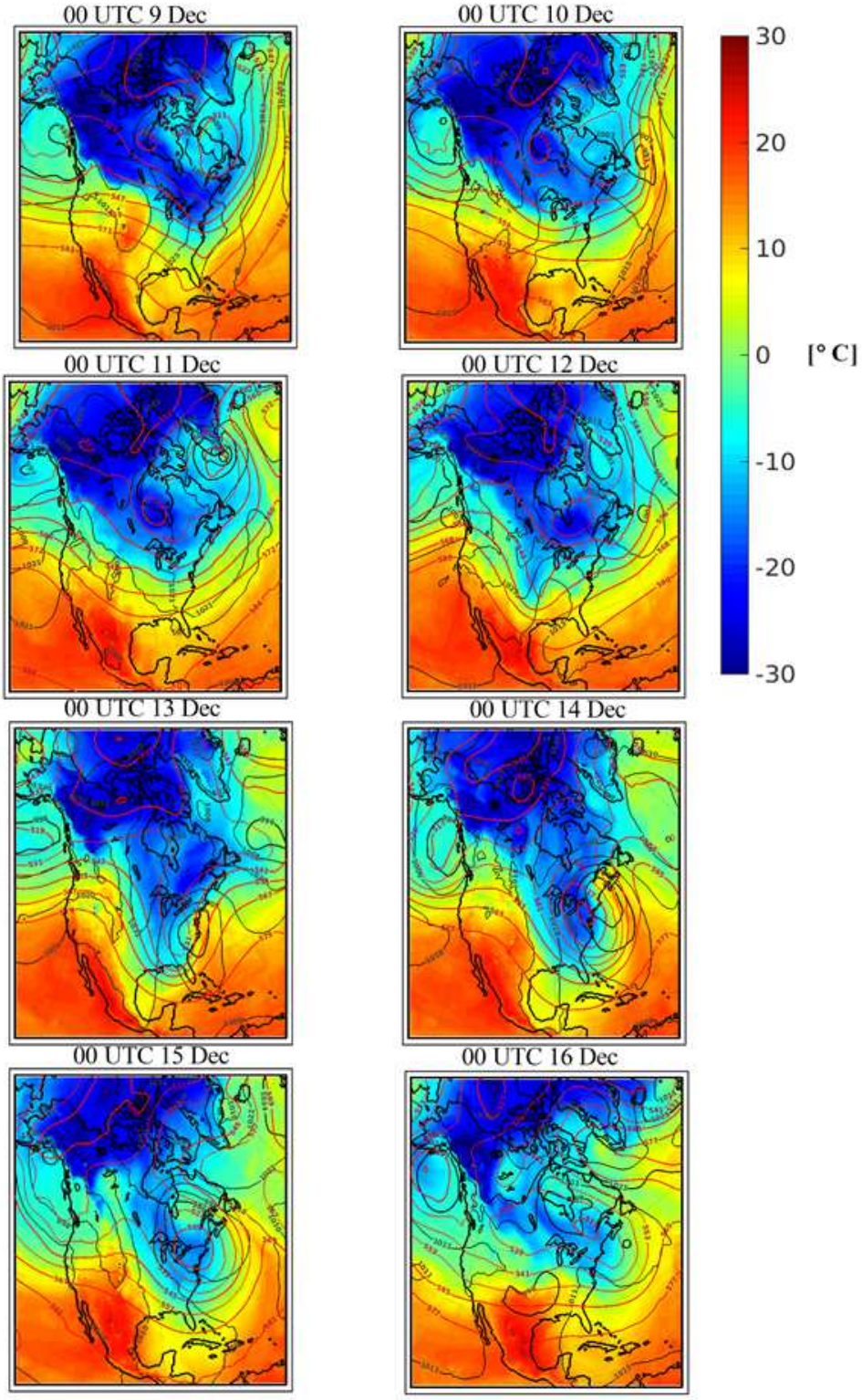

Figure 2

See the Manuscript Files section for the complete figure caption.

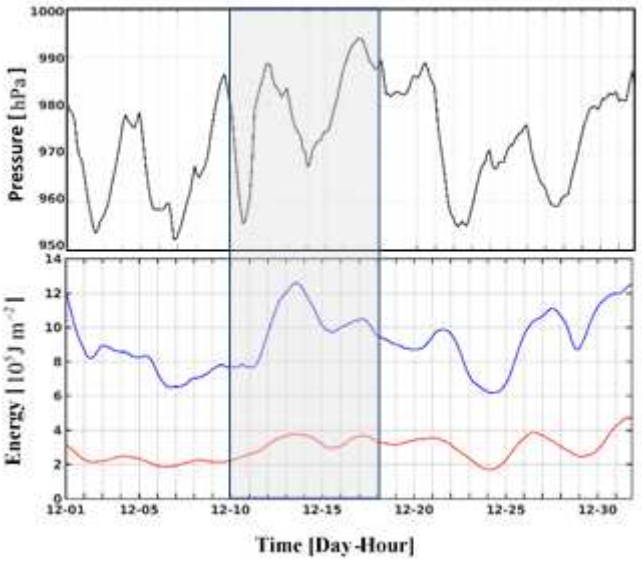

Figure 3

See the Manuscript Files section for the complete figure caption.

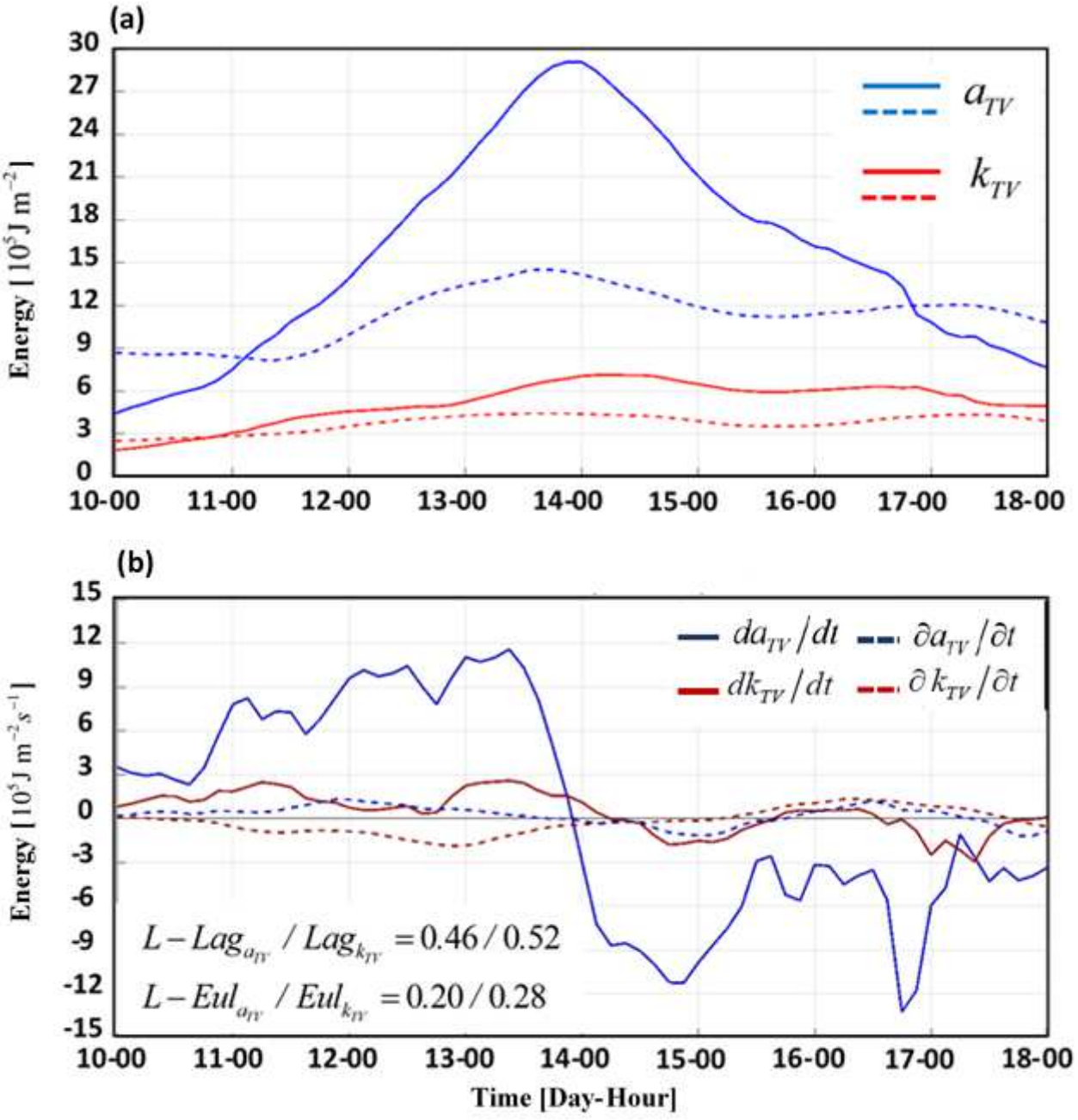

Figure 4

See the Manuscript Files section for the complete figure caption.

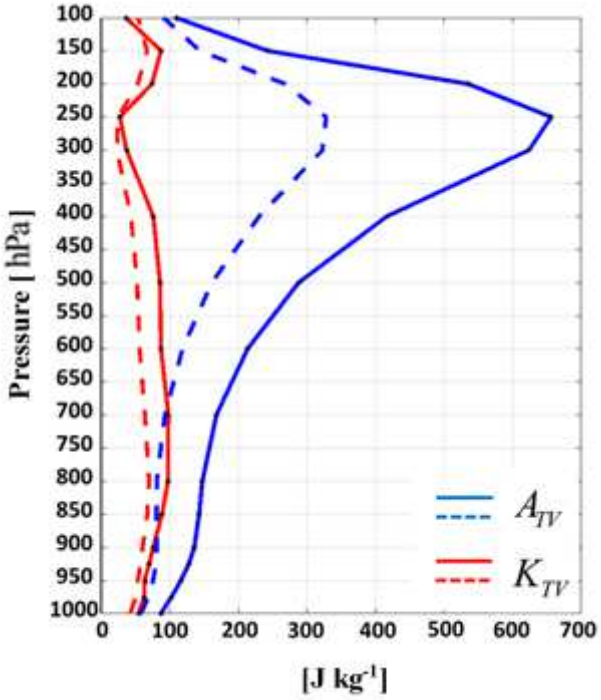

Figure 5

See the Manuscript Files section for the complete figure caption.

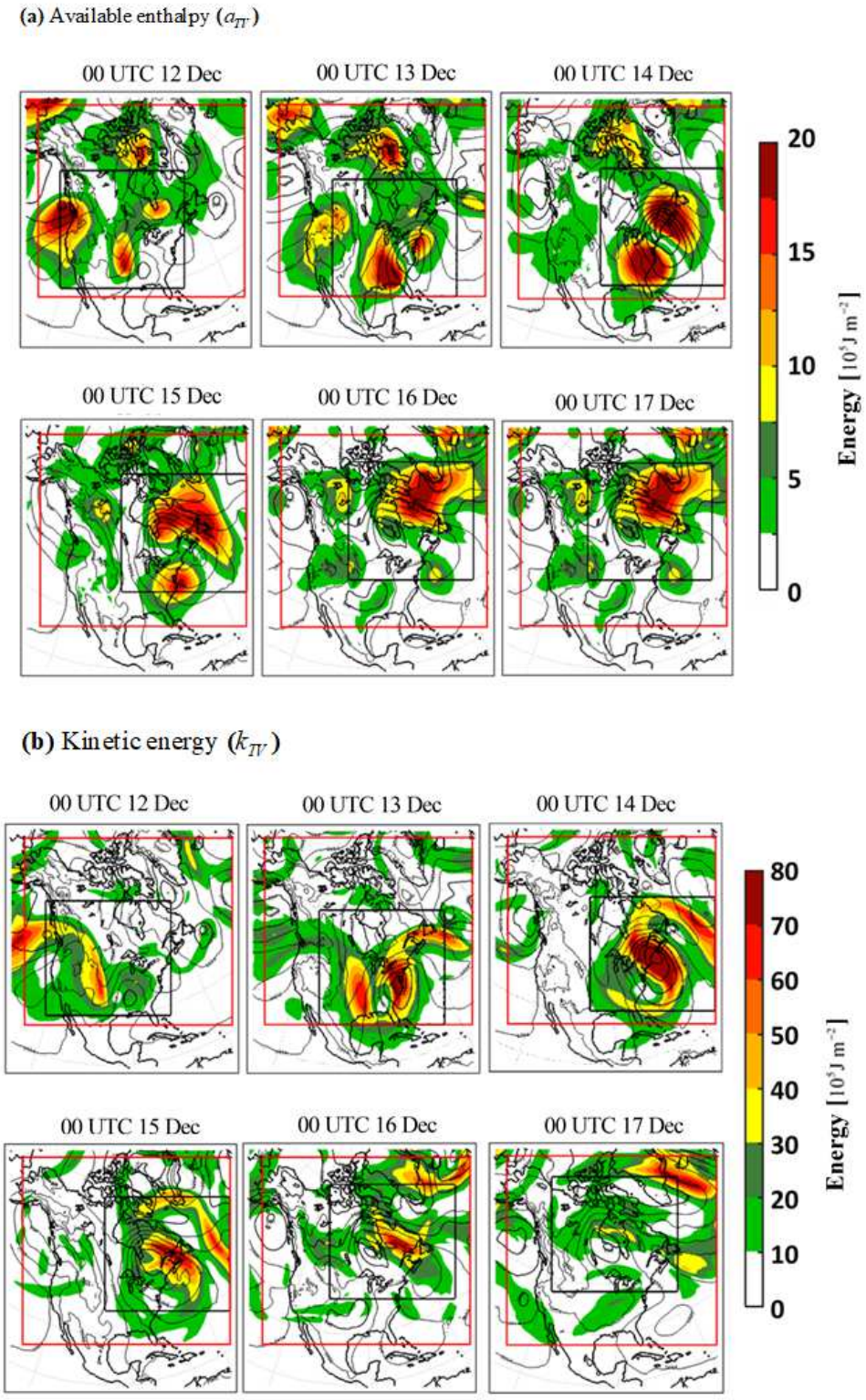

Figure 6

See the Manuscript Files section for the complete figure caption.

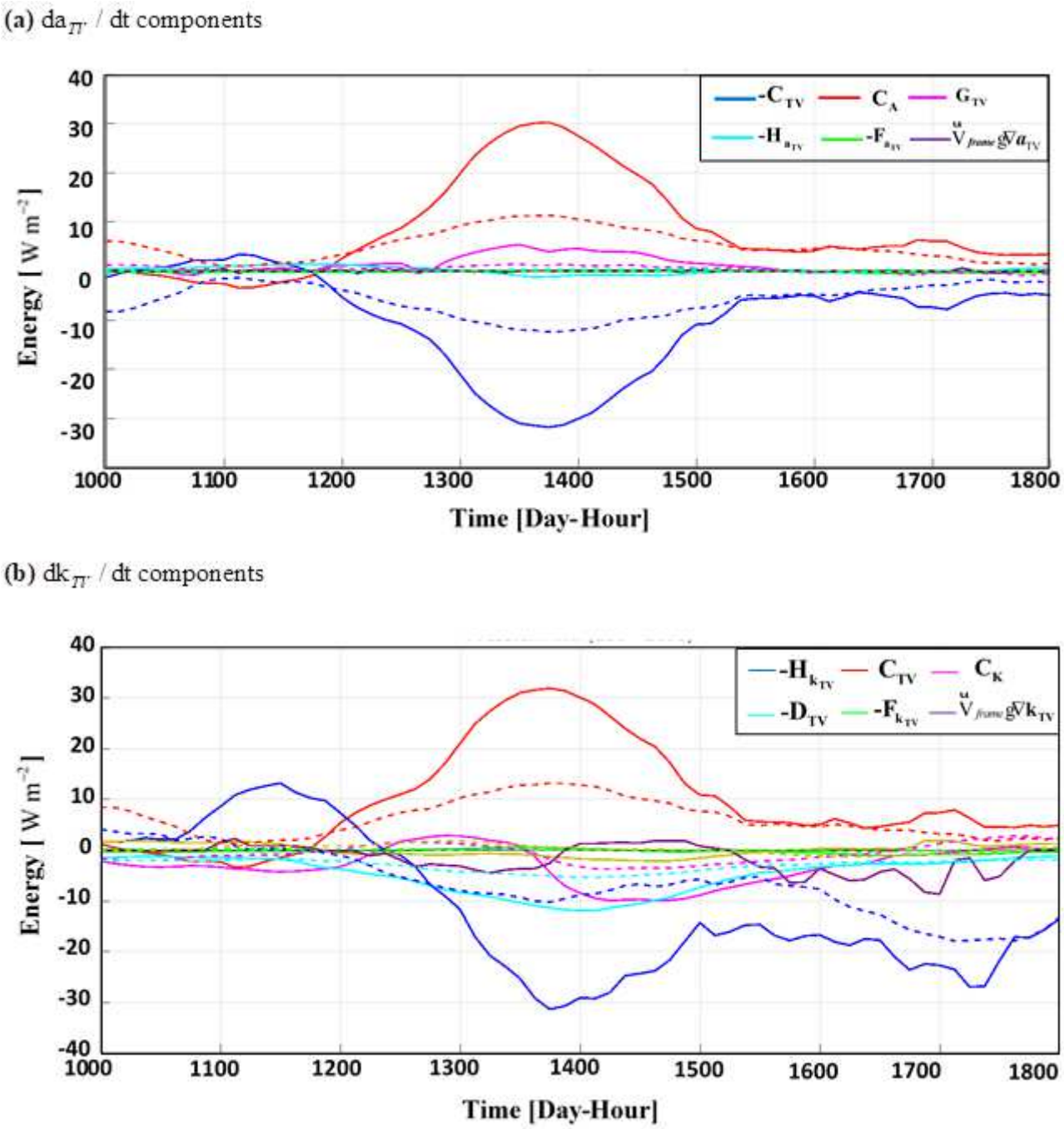

Figure 7

See the Manuscript Files section for the complete figure caption.

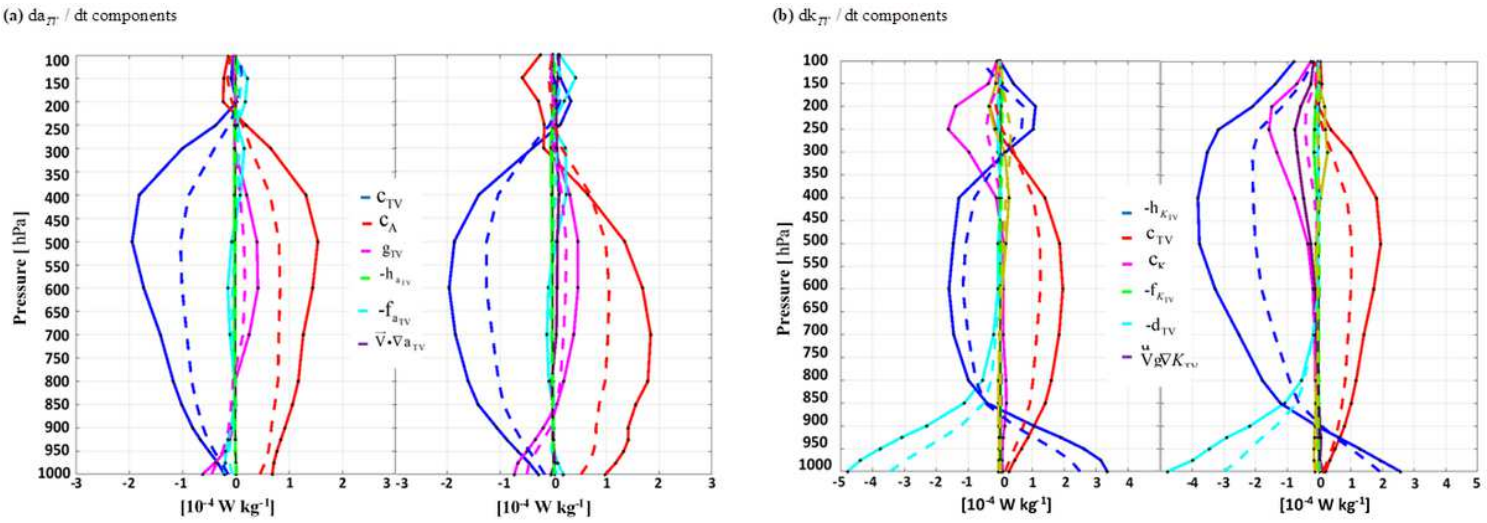

Figure 8

See the Manuscript Files section for the complete figure caption.

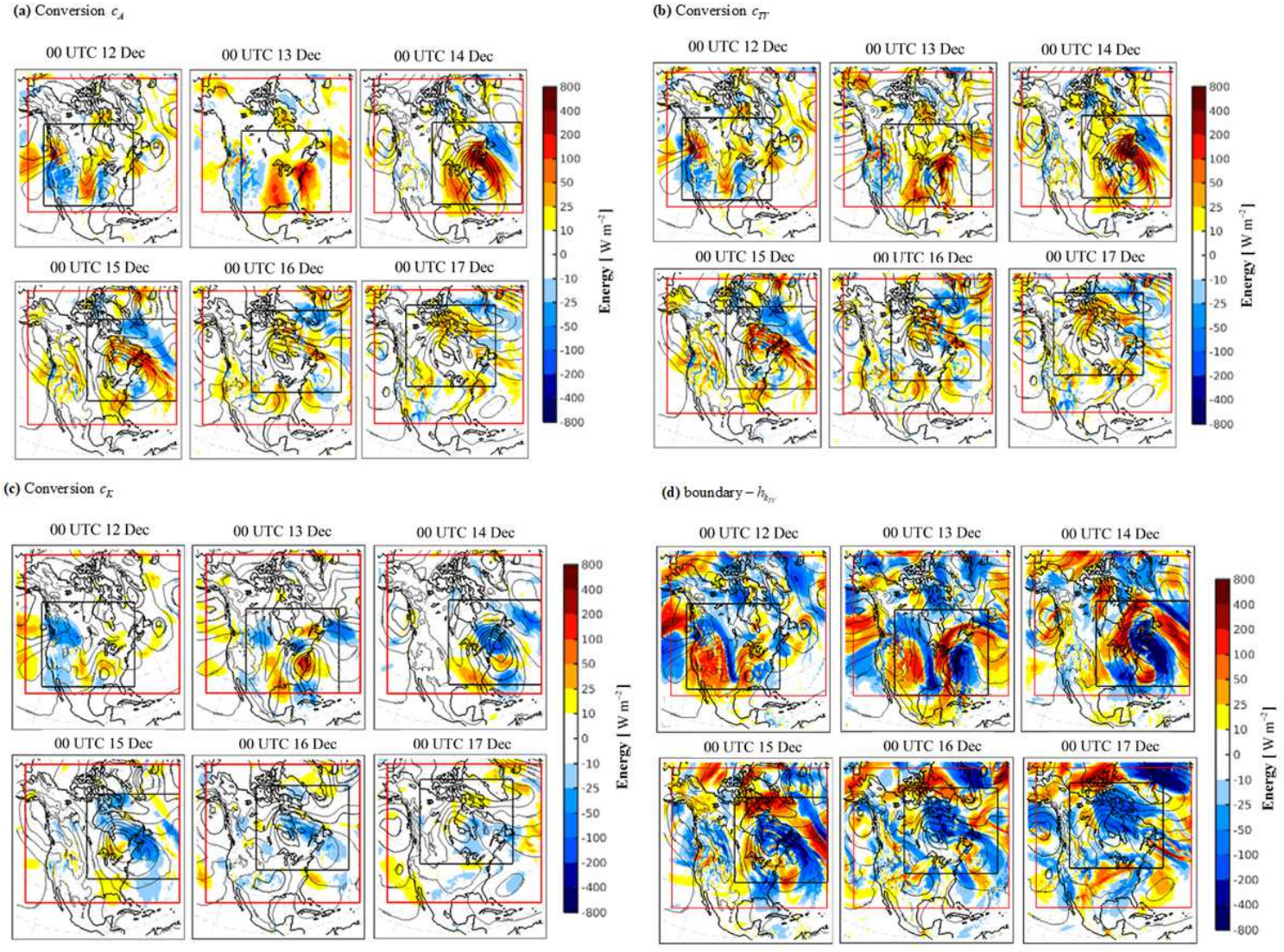

Figure 9

See the Manuscript Files section for the complete figure caption.

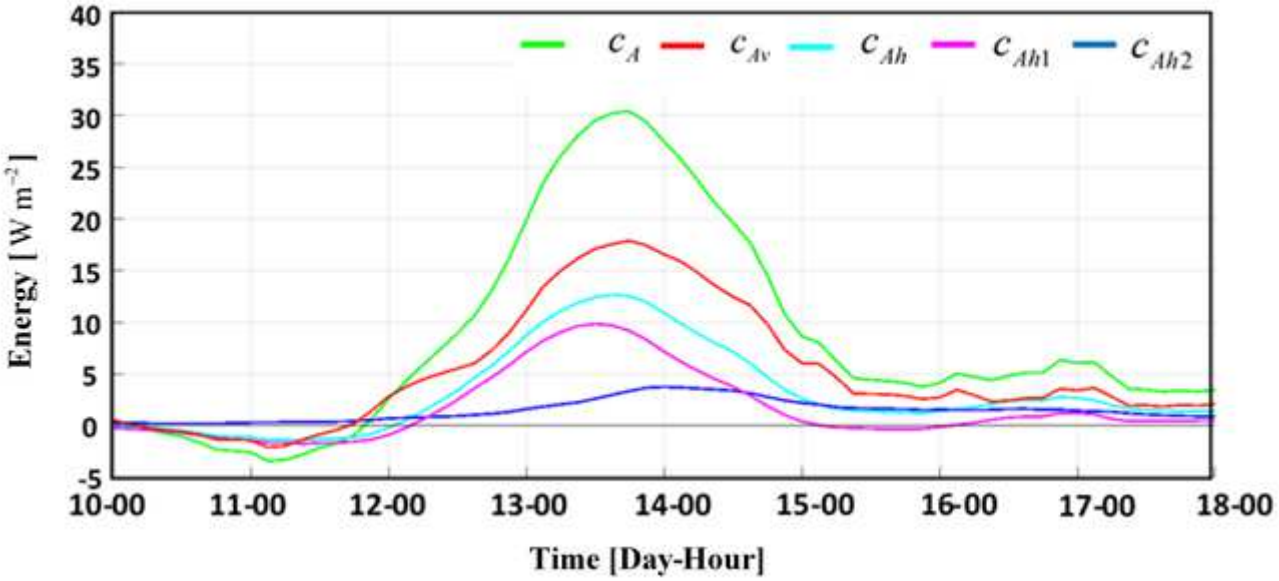

Figure 10

See the Manuscript Files section for the complete figure caption.

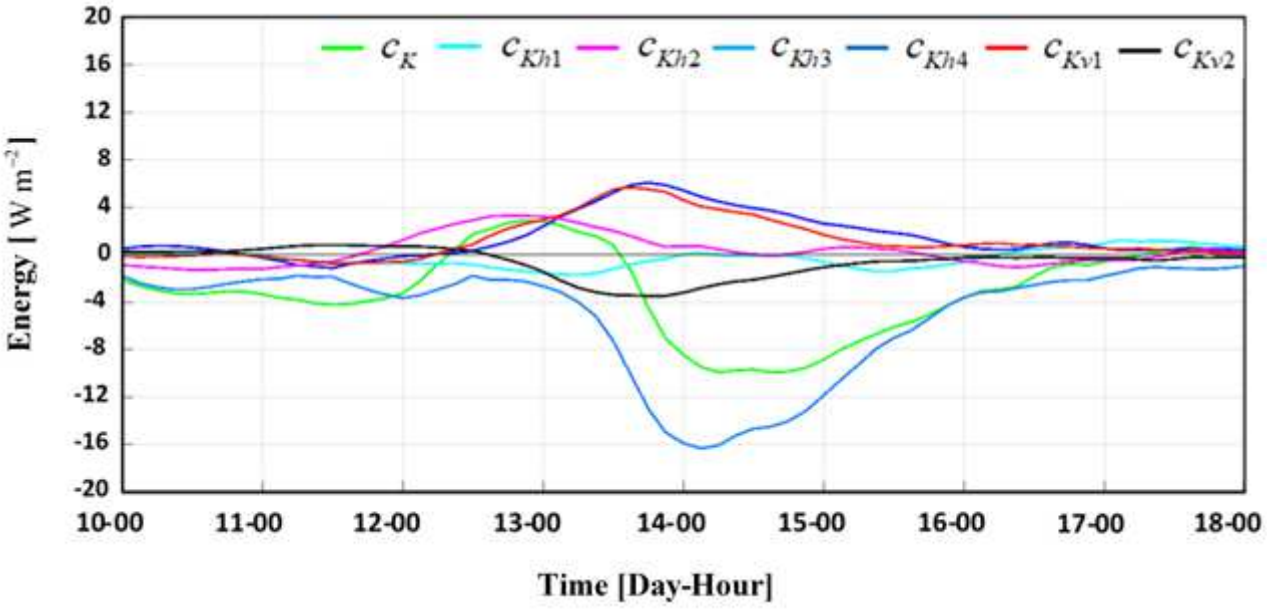

Figure 11

See the Manuscript Files section for the complete figure caption.

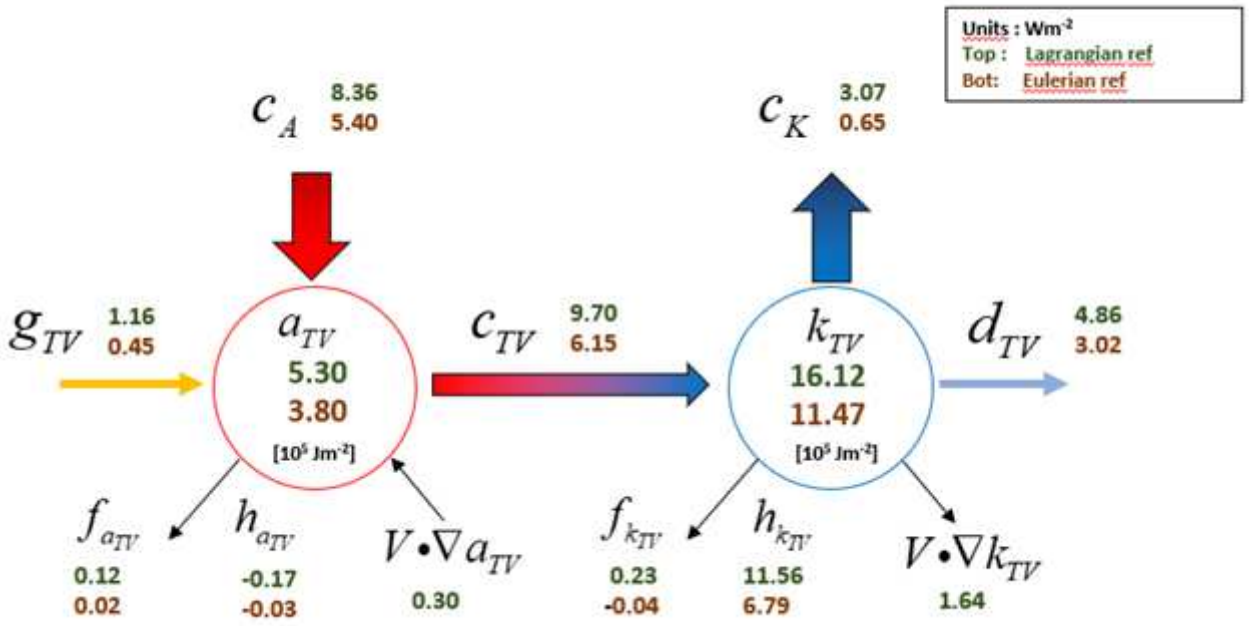

Figure 12

See the Manuscript Files section for the complete figure caption.

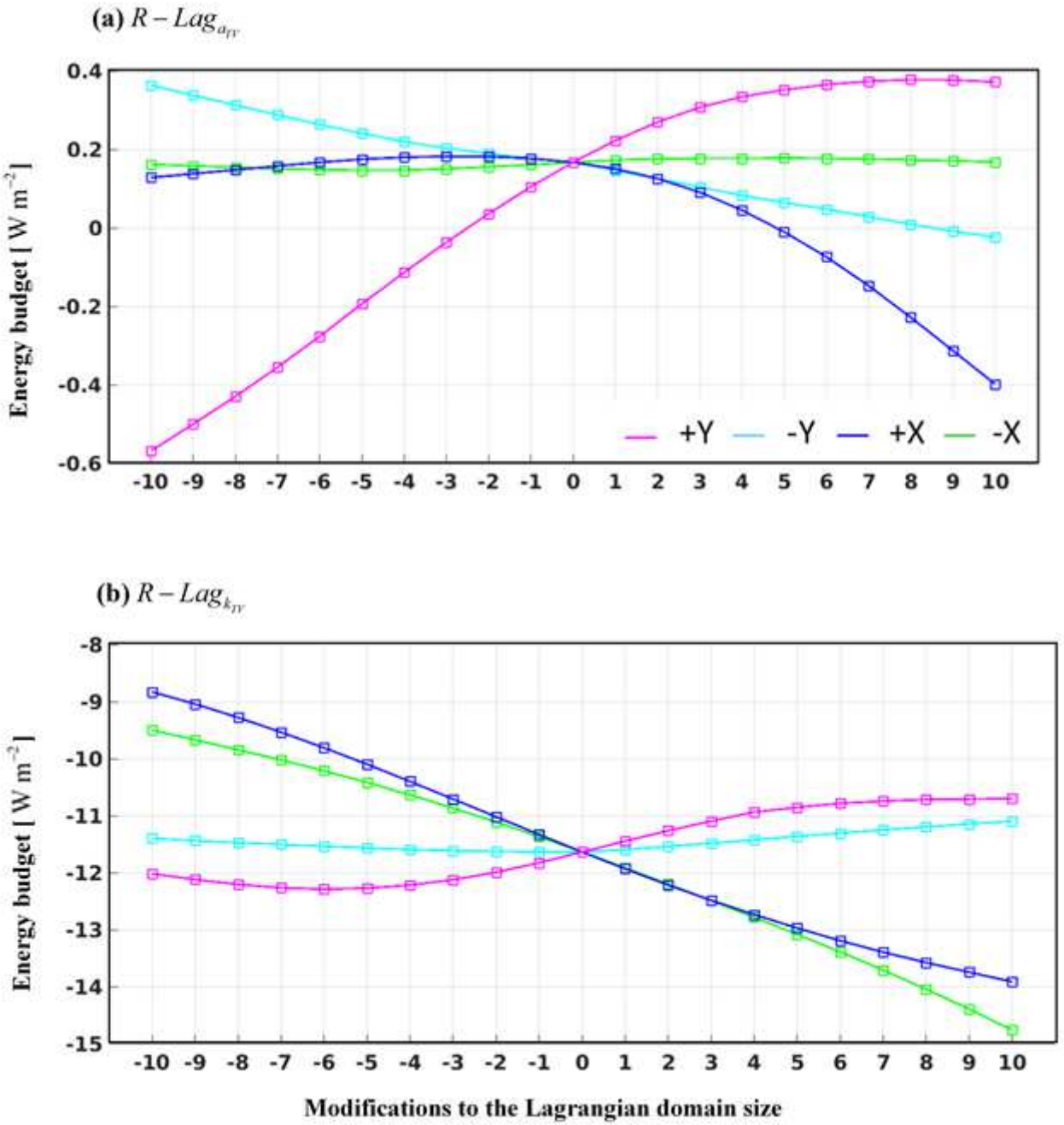

Figure 13

See the Manuscript Files section for the complete figure caption.

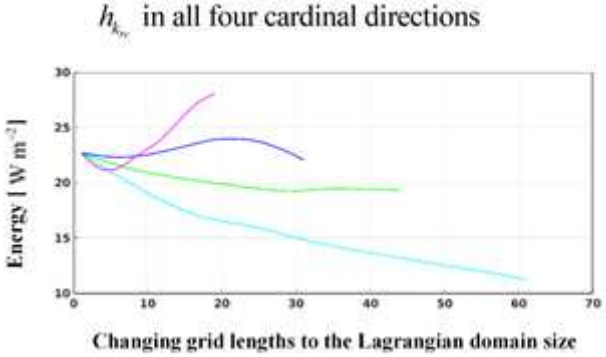

Figure 14

See the Manuscript Files section for the complete figure caption.

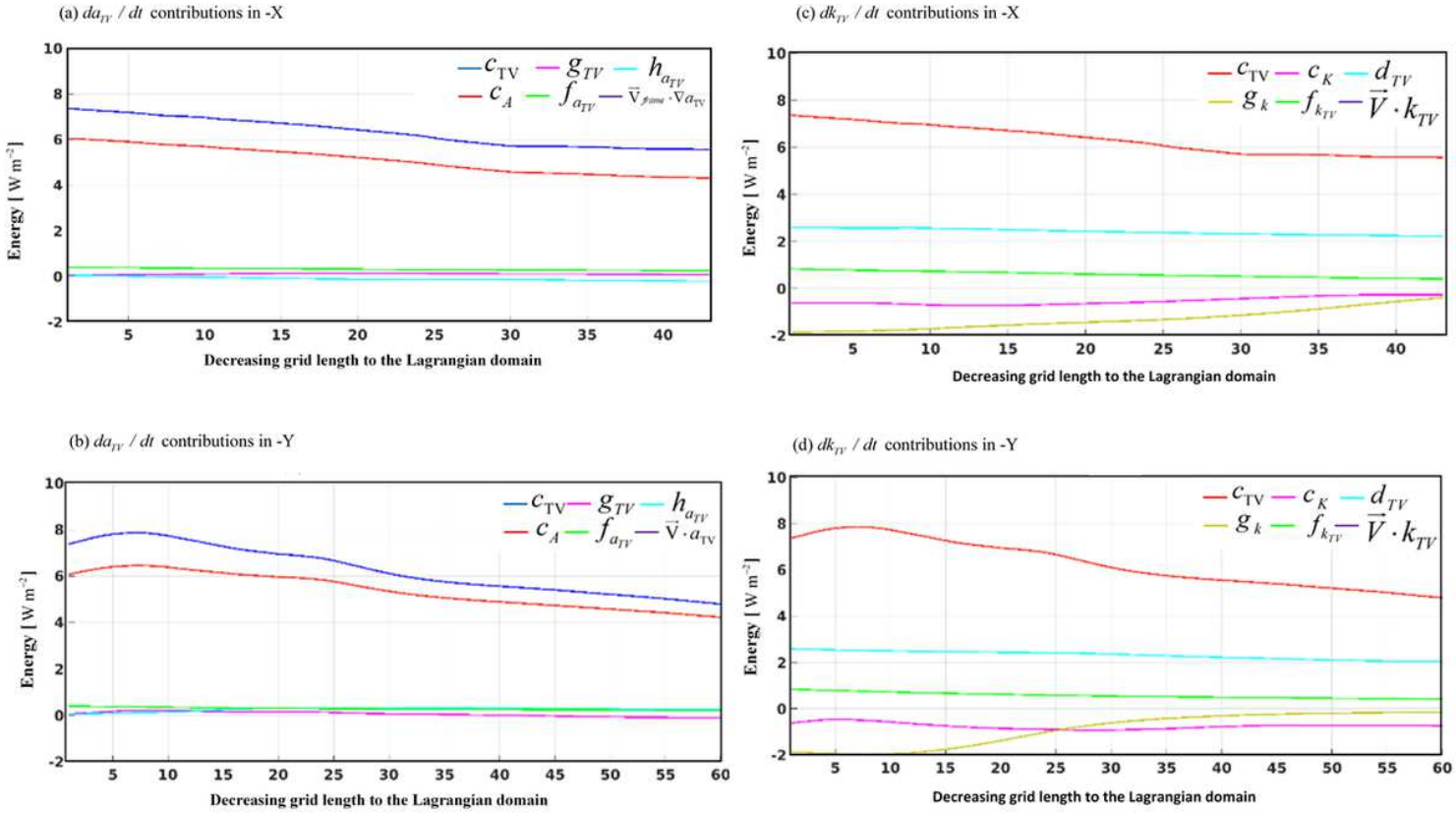

Figure 15

See the Manuscript Files section for the complete figure caption.